

# Supporting Information: Analysis of carbon-binder domain morphology and correlation to effective ion transport properties

Mrudula Prasad<sup>a,b</sup>, Benedikt Prifling<sup>c</sup>, Matthias Neumann<sup>c</sup>, Simon Hein<sup>a,b</sup>, Rares Scurtu<sup>d</sup>, Alice Hoffmann<sup>d</sup>, André Hilger<sup>e</sup>, Markus Osenberg<sup>e</sup>, Ingo Manke<sup>e</sup>, Margret Wohlfahrt-Mehrens<sup>d</sup>, Volker Schmidt<sup>c</sup>, Arnulf Latz<sup>a,b,f</sup>, Timo Danner<sup>a,b,\*</sup>

<sup>a</sup>*German Aerospace Center (DLR), Institute of Engineering Thermodynamics, Pfaffenwaldring 38-40, 70569 Stuttgart, Germany*

<sup>b</sup>*Helmholtz-Institut Ulm für Elektrochemische Energiespeicherung (HIU), Helmholtzstraße 11, 89081 Ulm, Germany*

<sup>c</sup>*Ulm University (UUlm), Institute of Stochastics, Helmholtzstraße 18, 89081 Ulm, Germany*

<sup>d</sup>*ZSW-Zentrum für Sonnenenergie- und Wasserstoff-Forschung Baden-Württemberg, Helmholtzstraße 8, 89081 Ulm, Germany*

<sup>e</sup>*Helmholtz-Zentrum Berlin für Materialien und Energie, Hahn-Meitner-Platz 1, 14109 Berlin, Germany*

<sup>f</sup>*Ulm University (UUlm), Institute of Electrochemistry, Albert-Einstein-Allee 47, 89081 Ulm, Germany*

---

## SI 1. Extracting the CBD domains

The 151 individual CBD domains were extracted via a Java script using the in-house software Geostoch [1]. The script parsed through each slice of the FIB-SEM data for  $128 \times 128 \times 128$  voxel<sup>3</sup> regions without any CAM within these boundaries. Figure SI-1 shows the extracted location of the CBD domains and the frequency distribution across the porosity range.

---

\*Corresponding author:

*Email address:* [timo.danner@dlr.de](mailto:timo.danner@dlr.de) (Timo Danner)

*URL:* <http://www.dlr.de/tt/en/> (Timo Danner)

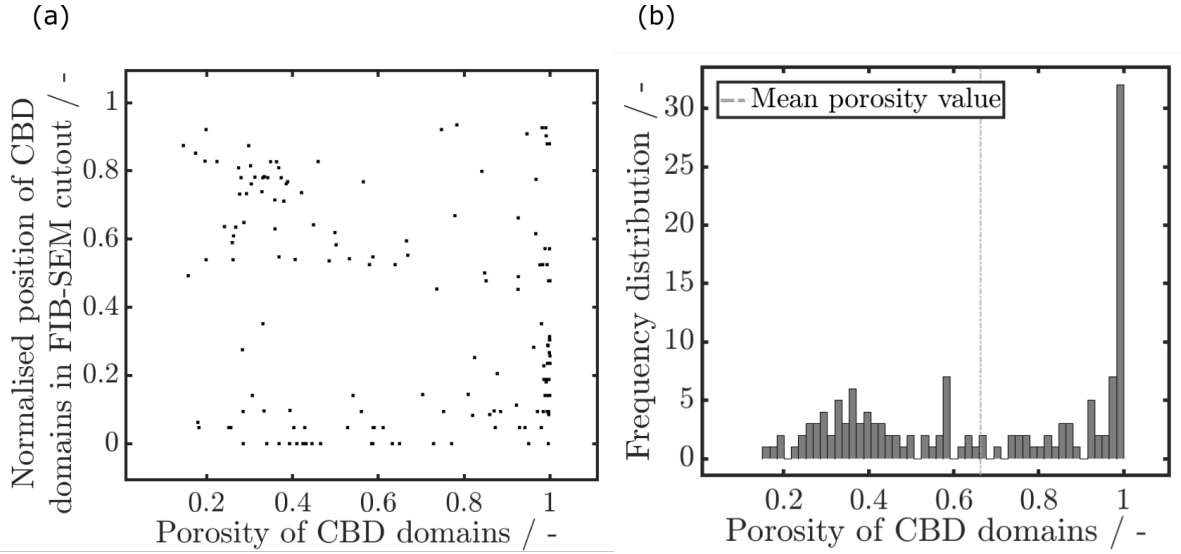


Figure SI-1: Shows (a) the location of the lower left-through-direction coordinate of the CBD domains normalised to the complete thickness of the FIB-SEM data, and (b) the frequency distribution of the extracted CBD domains.

## SI 2. Size of extracted domain

Dividing the whole 3D data set in subvolumes at different positions is a necessary step to quantify homogeneity of the subvolumes. The size of the subvolumes is motivated by different aspects:

- We chose it to be about an order of magnitude larger than the average pore size identified in the image data. Going smaller will further reduce statistics. Going much larger will include more regions with AM or pore only. Thereby, we again face the problem of assigning pore space to the CBD to quantify local porosities. We are facing this issue already in some regions with very high CBD porosity and we chose to filter CBD domains where the majority of the volume could not be assigned to CBD.
- We have complementary synchrotron image data on whole electrode samples and the voxel size of this data corresponds to the size of the extracted subvolumes. This allows correlation of gray-scale image data to density/porosity of the CBD. This is an important step to take this information to the electrode scale in future work.

## SI 3. Pre-processing of extracted CBD cutouts

The extracted CBD domains were pre-processed to ensure removal of artefacts from segmenting the original FIB-SEM data into the three materials. Domains whose solid fraction consisted of more than 10% isolated CBD clusters (consisting of less than 100 connected voxels) were disregarded from further analyses. Figure SI-2 shows that the

highly porous domains consist of solid CBD artefacts. Here the aim was not to remove all isolated clusters of solid CBD, but rather only those regions, which may have been incorrectly labelled as a CBD solid voxels. For e.g. small clusters of gray voxels floating in porous space.

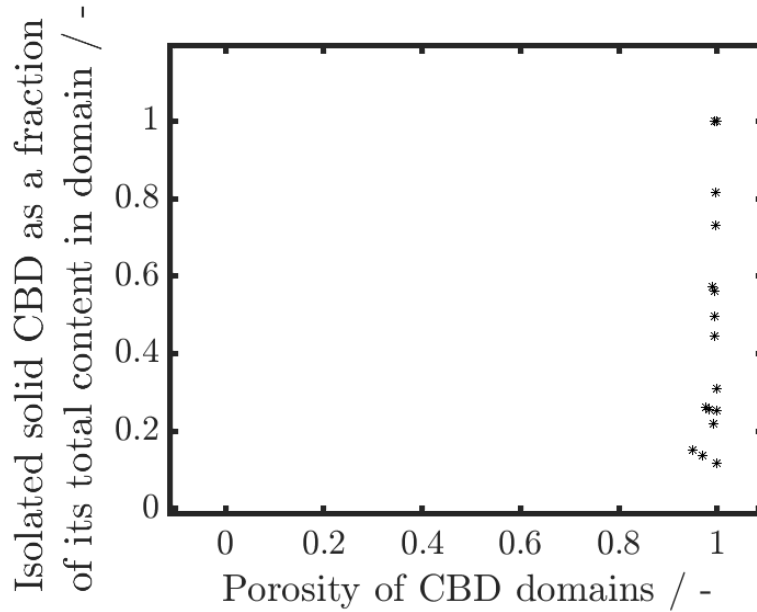


Figure SI-2: The fraction of solid CBD that is isolated in each domain. Majority of domains with porosities higher than 90% are disregarded as they primarily show free-floating/unconnected CBD domains. Such domains are not considered as belonging to CBD microstructure.

#### SI 4. Extending the CBD domains to include neighbouring pore space

It is obvious that the porosity of the CBD domain in Figure SI-3 (a) bordered in red does not belong to the CBD microstructure. In order to automatically remove such domains from further analyses, we extended the original CBD volume to include neighbouring voxels shown by the RGB-colour square. The number of neighbouring voxels for extension was elected via a voxelsize-independent study, i.e. when no further change in the number of pores centers in the inner CBD domain was noted once the pore network was extracted. So, they were extended to  $800^3$  voxels.

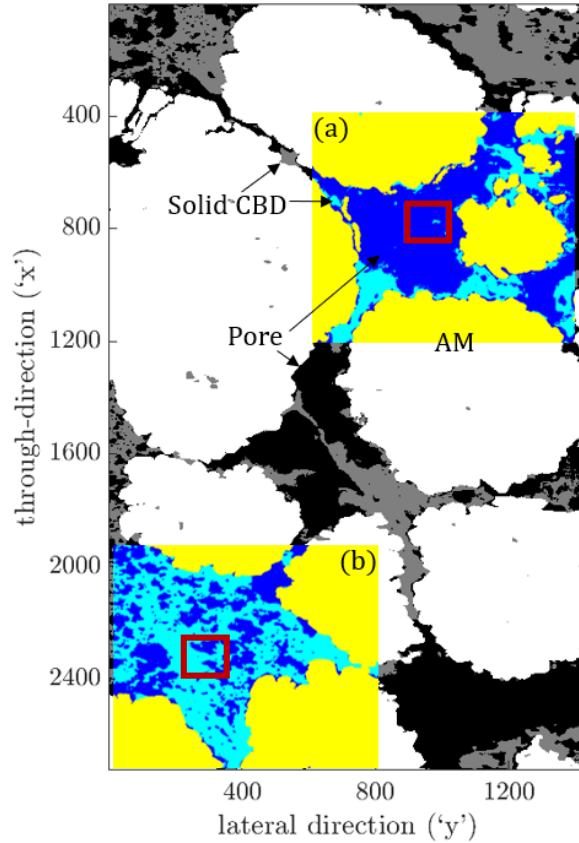


Figure SI-3: Shows the extension (in RGB colour scheme) of the inner CBD domain (in red) within the FIB-SEM slice (gray-scale) for morphological analyses. The extension includes all three material phases. In cyan/gray is the solid CBD, in dark blue/black the pore space and in yellow/white the CAM.

## SI 5. Segmenting and extracting the pore network

As mentioned in the main text, the SNOW2 toolbox [2] on PoreSpy was employed to segment and extract the pore network from image data. As an input one gives in a binarised image, where the solid voxels (CAM and CBD) have a false value and the porous regions (region to be segregated) gets a true value. As output, one gets the following parameters:

- the number of pore centers (i.e. pores) capturing the porous region. The pore coordinates were taken as the location of the peak in the centroid of the region. The peaks assigned to the pore centers are identified by applying a maximum filter with a Gaussian blur, for which a standard deviation of 0.4 was used to enable smoother identification of bright spots as pore centers, with a spherical structuring element with a radius of 4.

- the volume of each of these pores. The volume of a region was easily found by summing the number of voxels in the region.
- the equivalent diameters of the pores. Local distance map of just the pore region is used. This confines the pore body entirely inside its region before determining its diameter, creating a network of pores and throats.

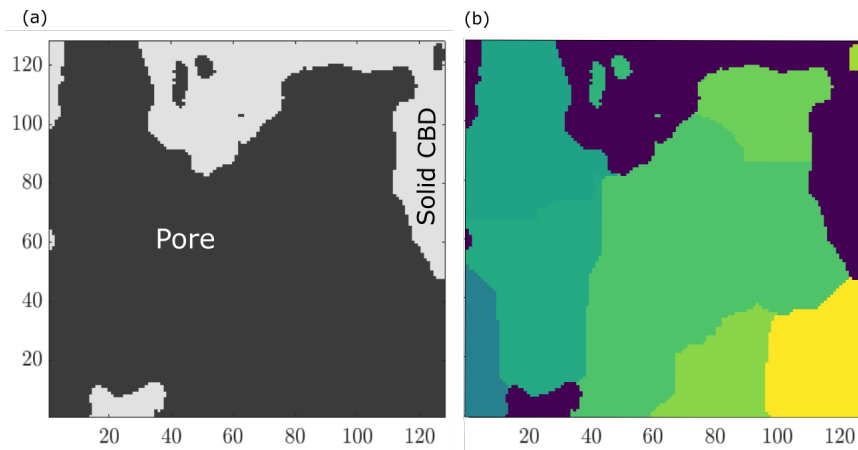


Figure SI-4: Inset (a) shows the a 2D-slice of CBD domain with 87% porosity. The corresponding segmentation of the pore space is given in segment (b). In the green/yellow colour scale is the pore space and in dark blue is the solid CBD. The colour scale is just to highlight the boundary between two pores.

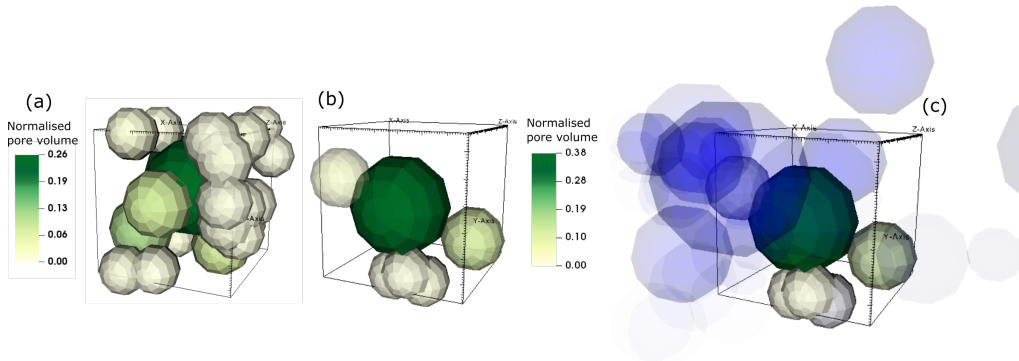


Figure SI-5: Extracted pore network within the original CBD domain boundaries with a porosity of 87%. The watershed is given in Figure SI-4. Pore network extracted when segmenting (a) just the CBD domain, and (b) and (c) the extended domain, without and with the excluded pore centers, respectively. In the green shade are the pores included, i.e. their pore centers and 50% of the pore volume lies within the bounding box. In blue shade are the excluded pores.

## SI 6. Methods to identify representative porosity range

As mentioned in Section Segmenting and extracting the pore network, the binarised image is first segmented into different pore regions using the watershed algorithm (see Figure SI-4). The extracted pore network is as seen in Figure SI-5. The metrics (Met.) applied to capture pore regions actually belonging to the CBD microstructure are as listed below. We distinguish between extended domains, upon which the segmentation was done (in RGB colours in Figure SI-3), and the CBD domain, upon which the metrics are actually applied (in red). Each of the metrics were applied at a microscale, i.e. to every single identified pore within each CBD domain.

Met. 1. The pore centers that did not lay within its original CBD boundaries (red area in Figure SI-3) were identified as not belonging to the CBD microstructure. These labelled regions were then deducted from the original CBD domain volume. After this volume reduction, the domains that had retained atleast 50% of their initial porosities were identified as representative.

Met. 2. Atleast 50% of each pore has to lie within the original CBD domain boundaries. When comparing Figures SI-1 and SI-6, we can see that the majority of the data points at higher porosity values (around 80% and above 90%) are not considered after this step. There is a higher probability of the pore centers to be lying out of the boundaries in the high porosity CBD domains. Majority of the domains are concentrated between 14% and 60% porosity. However, this step only accounts for the fraction of the pore volume intersecting with the domain boundaries and not the absolute value of the pore itself. This is then done in the next step.

Met. 3: The histogram Figure SI-7 summarises the pore volume distribution in all the shortlisted domains after the two previous metrics. As the data points are heavily skewed to the left, we assume that these are the pore volumes most representative of a CBD microstructure, and above this value, the volumes are given by CAM-CBD void space. So, we use the point (marked in a green diamond) where the pore diameter distribution starts to taper-off, as the maximum volume a CBD pore can have:  $0.7 \times 10^{-19} \text{ m}^3$ . At least 50% of each CBD domain should consist of pores whose volumes are lower than this value. As a further step, we used the segmentation algorithm to identify isolated pores, and all isolated pores with volumes lower than 0.05% of the domain are excluded. This gives us a minimum CBD radius of 60 nm. If the isolated pores are not removed, the smallest pore has a radius of 20 nm. Although it is possible, that CBD domains have isolated pore regions, these regions are non-conductive. We aimed to capture those domains where majority conducting pores are present. The frequency plot in Figure SI-8 shows the resulting porosity distribution after imposing the Met. (3). After all the metrics are applied, we retain about 17% of the initial structures. This results in porosities above 56% being discarded, however, the smallest porosity domain (14%) is still captured.

Additionally, the diameters of the chosen domains as extracted by the pore network algorithm is illustrated in Figure SI-9. The smallest pore diameter (60 nm) and the mode (100 nm) are in-line with that seen in literature [3, 4, 5], validating the metrics used.

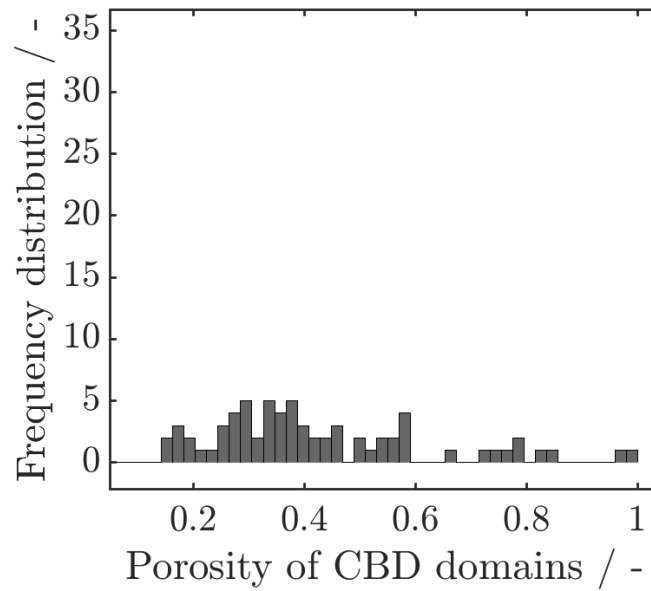


Figure SI-6: Histogram plot after Metrics (1.) and (2.) are established. The final porosity after Metrics (1.) and (2.) for pore positions and volumes, respectively, must lie within 50% of the original porosity. This results in the frequency distribution shown. The total number of valid data points drop to 68 from 151.

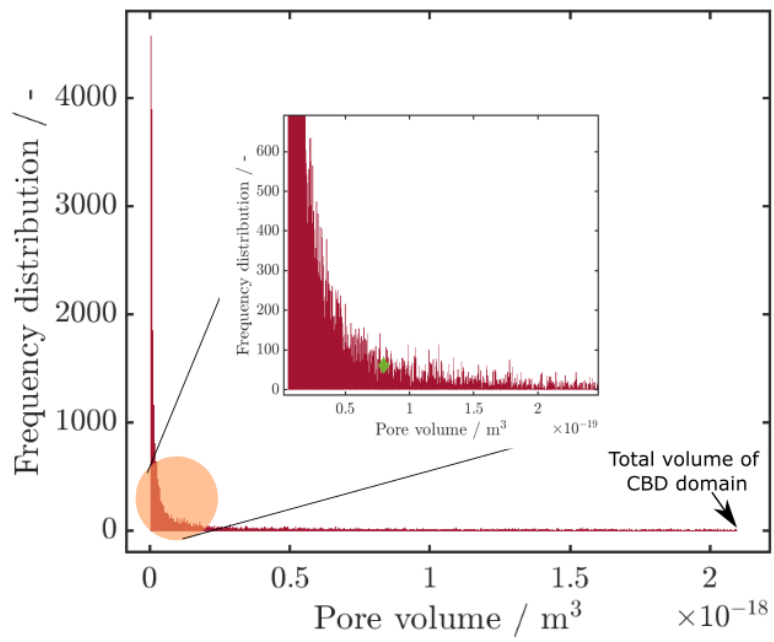


Figure SI-7: Shows the pore volume distribution considering all the pores in all the extended CBD domains upto a maximum volume which is the volume of the original CBD domain itself. Individual pores with volumes greater than  $0.7 \times 10^{-19} \text{ m}^3$  were disregarded.

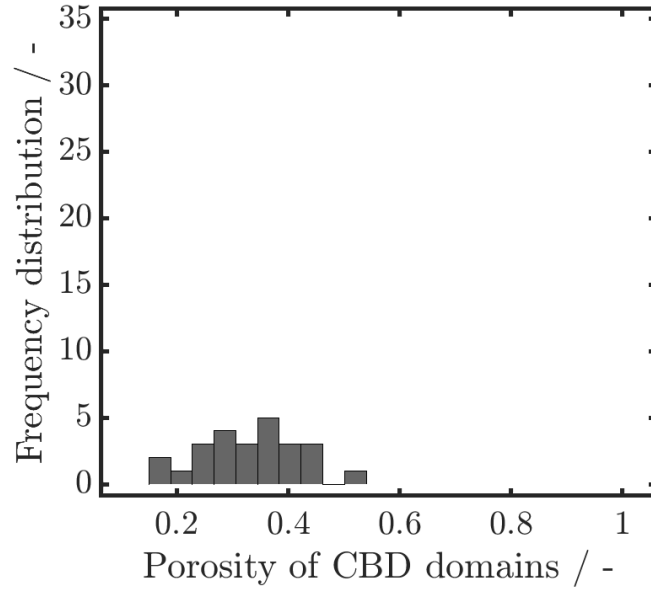


Figure SI-8: The final distribution of the porosities retained after the applied metrics Met. (1.), (2.) and (3.). The minimum porosity associated to the CBD microstructure is 14% as found in the original data, and maximum porosity is 56%.

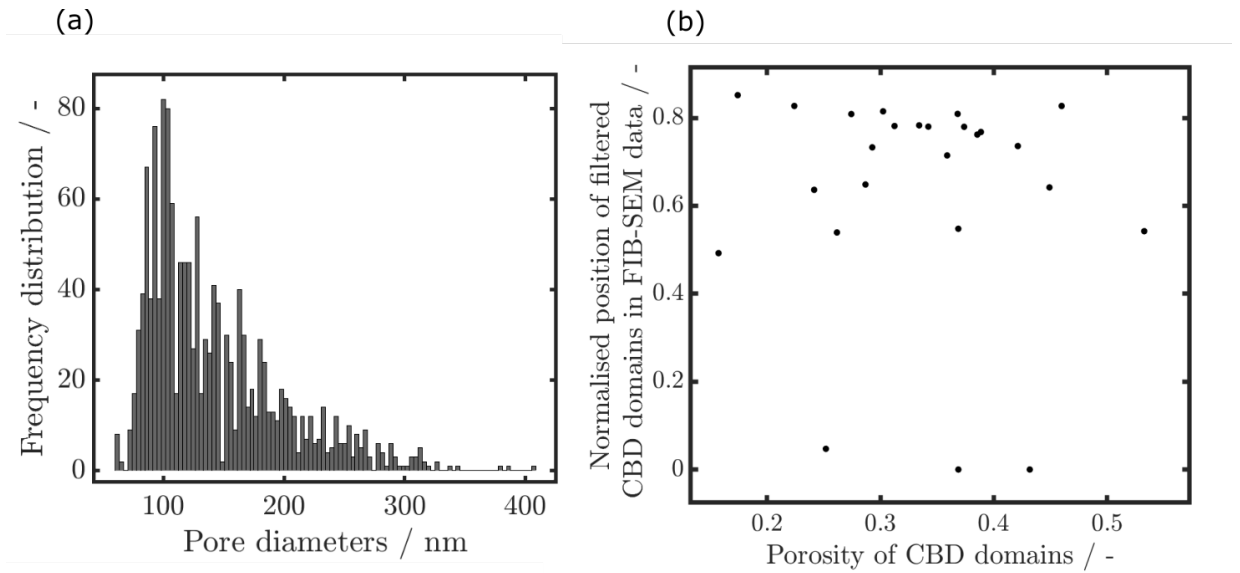


Figure SI-9: Shows (a) the distribution of the diameters when considering all the chosen domains after metrics Met. (1.), (2.) and (3.) The mode lies at approximately 100 nm. And (b) the location of the through-coordinate of the lower-left voxel of the final chosen CBD domains normalised across the thickness.

## SI 7. Determination of ion conductivity

To determine the effective conductivities of the CBD domains, the steady-state Poisson equation is solved with a constant current density boundary condition (as elucidated in [6]) using the BEST software [7], where  $\Delta x$  is the voxelsize,  $\phi$  is the applied potential difference,  $j$  is the resulting current, and  $\sigma_{eff}$  is the effective ion conductivity. Only the pore space (analogous to CBD porosity) was allowed to conduct ions. Lithium ions are distributed homogeneously in the electrolyte resulting in a concentration of 1 M.

$$\sigma_{eff} = j \frac{\Delta x}{\Delta \phi} \quad (\text{SI-1})$$

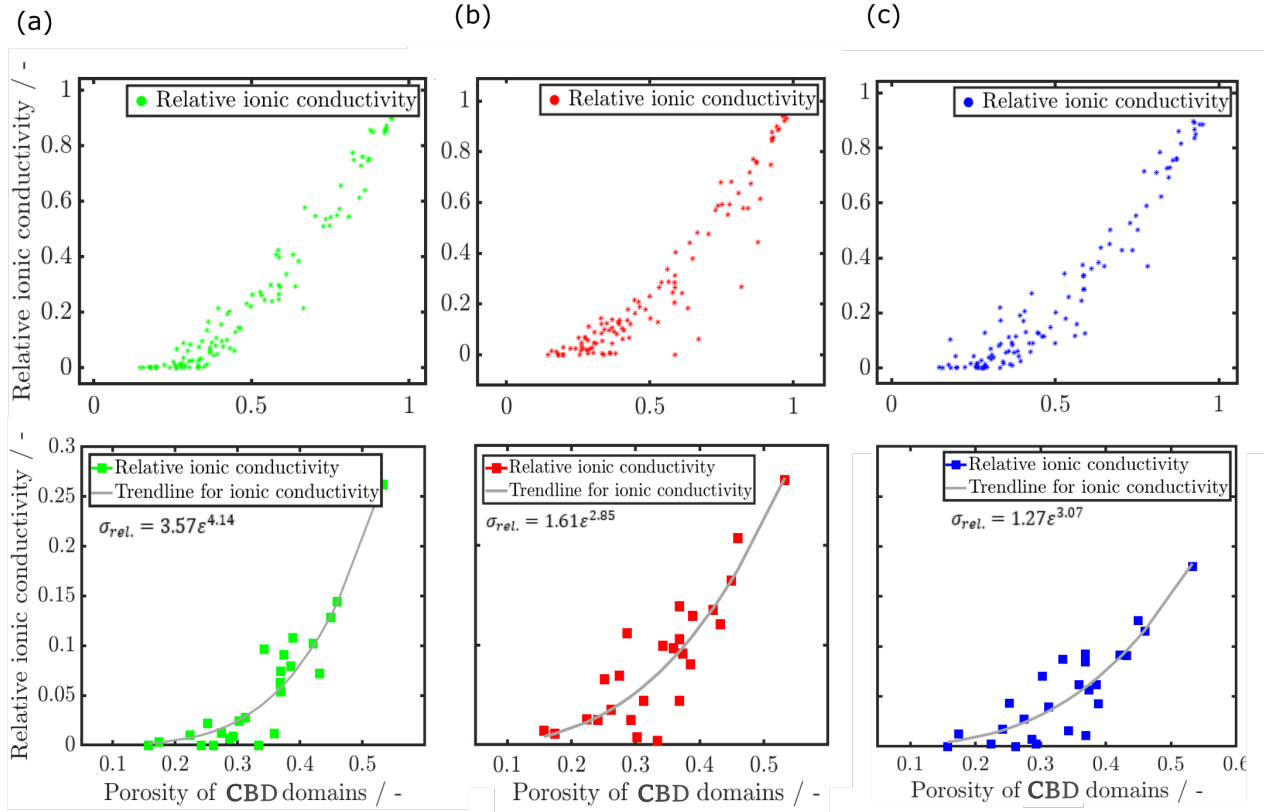


Figure SI-10: The first row shows the full data set of the ion conductivity data in each direction of flow, and the second row shows the conduction in the final chosen domains in each direction of flow. Column (a) is the x-direction of flow (i.e. the through-direction), (b) the y, and (c) the z-direction of flow.

## SI 8. Electronic conductivity

The Figure SI-11 shows the (a) dependence of the electronic conductivity on the porosity of all the extracted CBD domains, compared to (b) just the final filtered CBD domains. Here, only the solid phase is conducting.

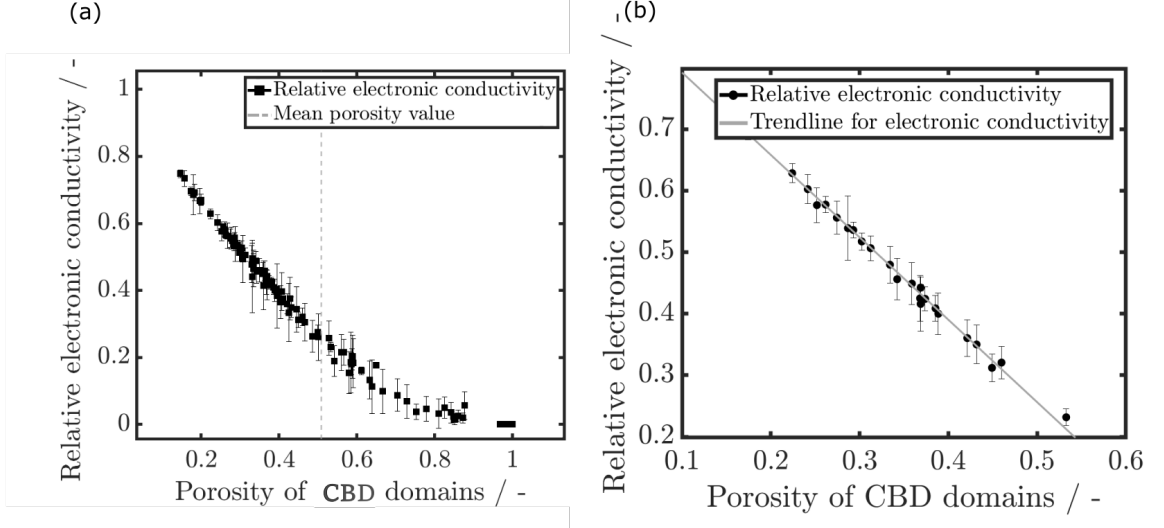


Figure SI-11: (a) Shows the dependency of the relative electronic conductivity on the entire porosity range of the CBD domains. (b) Shows the relative electronic conductivity in the final filtered domains. The best fit to the data is a linear trendline of the form:  $\kappa_{rel.} = 1.34\epsilon + 0.93$ , where  $\kappa_{rel.}$  is the effective electronic conductivity within the CBD phase, where only the solid carbon material is electronically conducting.

## SI 9. Validation of the chosen porosity range

The focus of this work is first on presenting the method on resulting correlation for CBD morphology which has not yet been employed in the literature. Direct local measurements of electronic conductivity are challenging, yet maybe feasible with AFM; which would still not provide bulk values, nor insight into the porosity of the local measured volume. We are also not aware of direct measurements of local ionic transport properties. Therefore, combining imaging, and electrode scale electrochemical characterization (impedance spectroscopy on symmetric cells and rate tests) with simulation tools in data-driven approaches might be a pathway to indirectly characterize and validate the derived CBD properties, and is something we are working on.

In lieu of the aforementioned validation approach, we have availed the average tortuosity and porosity values derived from the current study, and applied it to an electrode where the CBD was reconstructed using neural networks. More information to the reconstruction is provided in Prifling et al. [8]. They assumed a homogeneous porosity of the CBD phase for the electrode, and fit its ionic tortuosity until the simulations agreed with

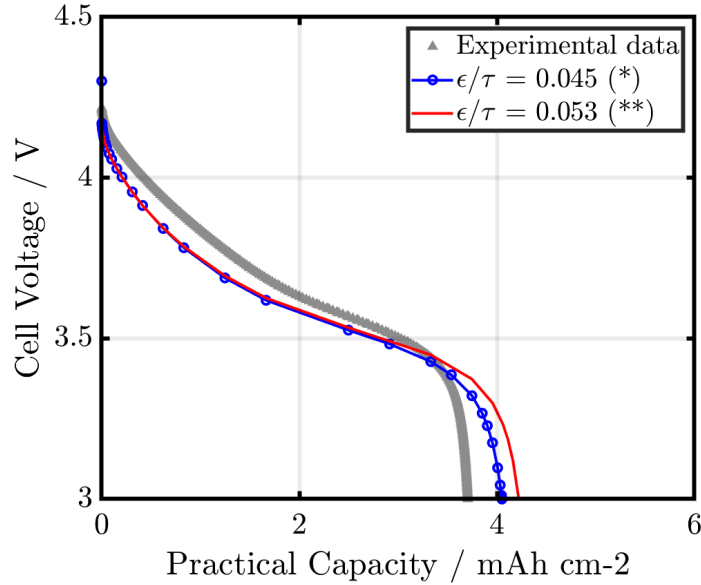


Figure SI-12: Shows the comparison between the experimental data and the two studies for single-layer electrodes at  $6 \text{ mA/cm}^2$  current, both of which use the same electrode, where the CBD reconstructed via neural networks [8]: (\*) simulated with a homogeneous tortuosity (11.1) and porosity (50%) as determined in [8]; (\*\*) same electrode as in (\*) but with the mean tortuosity (6.41) and porosity (33.68%) as determined in this study.

the experimental half-cell discharge data. We can see from Figure SI-12 that, the mean values from the current study overestimate the delivered capacity slightly, but predicted capacity is still agreeable with the experimental data.

Identified values from this study suggest that, the method using a neural network to extract macroscopic CBD distribution and the resulting fitted mean effective transport parameter are closest to the mean values identified in this work.

## SI 10. Specific surface area

In this section, the specific surface areas (SSA) between the solid CBD and pore, as well as the solid CBD and CAM is presented (see Figure SI-13). Pores identified as not belonging to the CBD microstructure are isolated for the purposes of this calculation, and are thus labelled as macropores in the figure legend. As there is no CAM within the bounds of the  $128^3$  voxels cutout, the domains are engulfed with a single-voxel thick foreign ID corresponding to CAM.

With increasing porosity, the probability that the outer pores belong to the macroporous space is higher. This reduces the contact between the engulfing CAM ID and

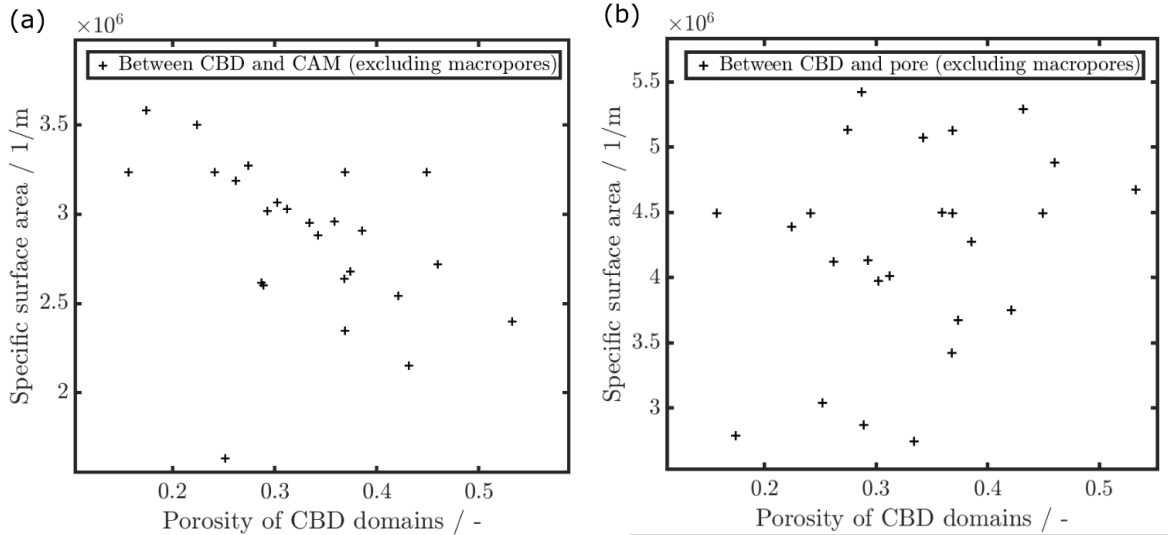


Figure SI-13: Specific surface area between (a) CBD and CAM. To determine this, the cubic  $128^3$  voxels domains were enveloped in one-voxel thick CAM ID. (b) CBD and pore space. For both (a) and (b), the pores not belonging to the CBD microstructure were not considered.

the solid CBD. There is a sharp decrease in the SSA for the domain with a porosity of approximately 25%. Removing the macropores likely resulted in large isolated regions of solid CBD, reducing the contact to CAM.

From Figure SI-13 (b), there seems to be no dominant relationship between the inner conductive pore space of the CBD microstructure, and its solid CBD fraction. The location of the pores removed greatly influences the contact points between the two phases.

## References

- [1] J. Mayer, A time-optimal algorithm for the estimation of contact distribution functions of random sets, *Image Analysis and Stereology* 23 (2011) 177–183.
- [2] J. T. Gostick, Versatile and efficient pore network extraction method using marker-based watershed segmentation, *Physical Review E* 96 (023307) (2017).
- [3] S. Vierrath, L. Zielke, R. Moroni, A. Mondon, D. R. Wheeler, R. Zengerle, S. Thiele, Morphology of nanoporous carbon-binder domains in Li-ion batteries - A FIB-SEM study, *Electrochemistry Communications* 60 (2015) 176–179.
- [4] J. K. Mayer, H. Bockholt, A. Kwade, Inner carbon black porosity as characteristic parameter for the microstructure of lithium-ion electrodes and its effect on physical and electrochemical properties, *Journal of Power Sources* 529 (231259) (2022).
- [5] S. Radloff, L. S. Kremer, A. Hoffmann, M. Wohlfahrt-Mehrens, Characterization of structured ultra-thick  $\text{LiNi}_{0.6}\text{Co}_{0.2}\text{Mn}_{0.2}\text{O}_2$  lithium-ion battery electrodes by mercury intrusion porosimetry, *Materials Today Communications* 28 (2021) 102549.
- [6] T. Knorr, S. Hein, B. Prifling, M. Neumann, T. Danner, V. Schmidt, A. Latz, Simulation-based and data-driven techniques for quantifying the influence of the carbon binder domain on electrochemical properties of Li-ion batteries, *Energies* 15 (2022) 7821.

- [7] Fraunhofer Institute for Industrial Mathematics (ITWM), BEST - Battery and Electrochemistry Simulation Tool (2020).  
URL <http://itwm.fraunhofer.de/best>
- [8] B. Priffling, M. Neumann, S. Hein, T. Danner, E. Heider, A. Hoffmann, P. Rieder, A. Hilger, M. Osenberg, I. Manke, M. Wohlfahrt-Mehrens, A. Latz, V. Schmidt, Quantitative comparison of different approaches for reconstructing the carbon-binder domain from tomographic image data of cathodes in lithium-ion batteries and its influence on electrochemical properties, *Energy Technology* 11 (5) (2023) 2200784.